Turbulence, Heat and Mass Transfer 10

Can we hit the ultimate regime of thermal turbulence using LES simulations at low Prandtl numbers?

F.X.Trias[1], A.Gorobets[2], A.Oliva[1]

[1] *Heat and Mass Transfer Technological Center, Technical University of Catalonia*
C/Colom 11, 08222 Terrassa (Barcelona) *E-mail: francesc.xavier.trias@upc.edu*

[2] *Keldysh Institute of Applied Mathematics, 4A, Miusskaya Sq., Moscow 125047, Russia*

Abstract – In this work, we aim to shed light on the following research question: *can we hit the ultimate regime of thermal turbulence using large-eddy simulations (LES) at low Prandtl numbers?* This is motivated by our recent findings showing the reliability of LES techniques at low-Pr where no subgrid heat flux activity is expected. Hence, we are carrying out a set of LES simulations of a Rayleigh–Bénard configuration at $Pr = 0.005$ (liquid sodium) using two levels of refinement. According to our estimations the two highest Rayleigh numbers (2.25×10^{10} and 7.14×10^{10}) are located in the region of the $\{Ra, Pr\}$-phase space where the $Nu \propto Ra^{1/2}$ power-law scaling of the ultimate regime should be observed. This asymptotic regime was theoretically predicted by Kraichnan in the early 60s; however, despite the great efforts devoted, it still remains elusive.

1. Introduction

Buoyancy-driven flows have always been an important subject of scientific studies with numerous applications in environment and technology. The most famous example thereof is the thermally driven flow developed in a fluid layer heated from below and cooled from above, *i.e.* the Rayleigh-Bénard convection (RBC). Figure 1 displays two examples of turbulent air-filled RBC configurations. It constitutes a canonical flow configuration that resembles many natural and industrial processes, such as solar thermal power plants, indoor space heating and cooling, flows in nuclear reactors, electronic devices, and convection in the atmosphere, oceans and the deep mantle.

In the last decades significant efforts, both numerically and experimentally, have been directed at investigating the mechanisms and the detailed scaling behavior of the Nusselt number as a function of Rayleigh and Prandtl numbers in the general form $Nu \propto Ra^{\gamma} Pr^{\beta}$ [1]. In this regard, Figure 2 shows the predictions of the Nu-number based on the classical Grossmann-Lohse (GL) theory [2] and its subsequent corrections [3, 4] where different scaling regimes, characterized by their corresponding exponents γ and β, are identified. Assuming this power-law scalings and following the same reasoning as in Ref. [5] leads to the estimations for the number of grid points shown in Figure 5 (top). This corresponds to mesh resolution requirements for direct numerical simulation (DNS) and it clearly explains why nowadays DNS of RBC is still limited to relatively low Ra-numbers [1]. However, many of the above-mentioned applications are governed by much higher Ra numbers, located in the region of the $\{Ra, Pr\}$ phase space where the thermal boundary layer becomes turbulent (*i.e.* below the black dash-dotted line in Figure 2). This region corresponds to the so-called asymptotic Kraichnan or ultimate regime of turbulence [6], with $\gamma = 1/2$. On the other hand, reaching such Ra-numbers experimentally while keeping the basic assumptions (Boussinesq approximation, adiabaticity of the closing

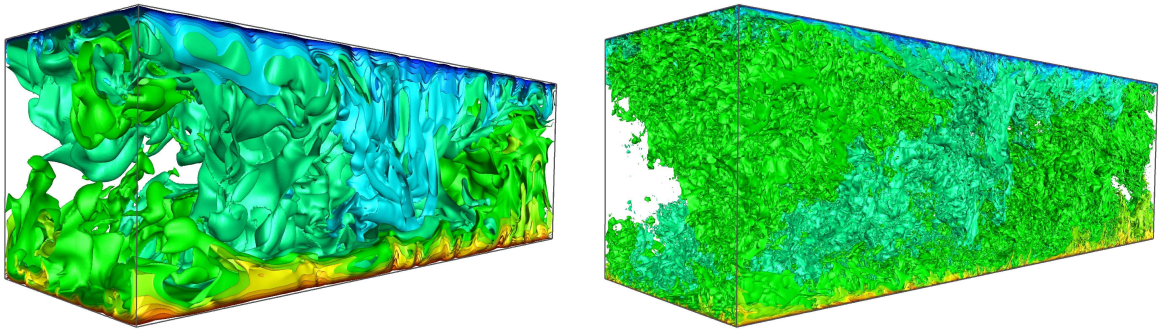

Figure 1: Visualization of instantaneous temperature fields of an air-filled (Pr $= 0.7$) RBC at at $Ra = 10^8$ (left) and $Ra = 10^{10}$ (right). Results correspond to the statistically steady state of the DNS simulations studied in Refs. [5, 7] using meshes of $400 \times 208 \times 208 \approx 17.3M$ and $1024 \times 768 \times 768 \approx 604M$, respectively.

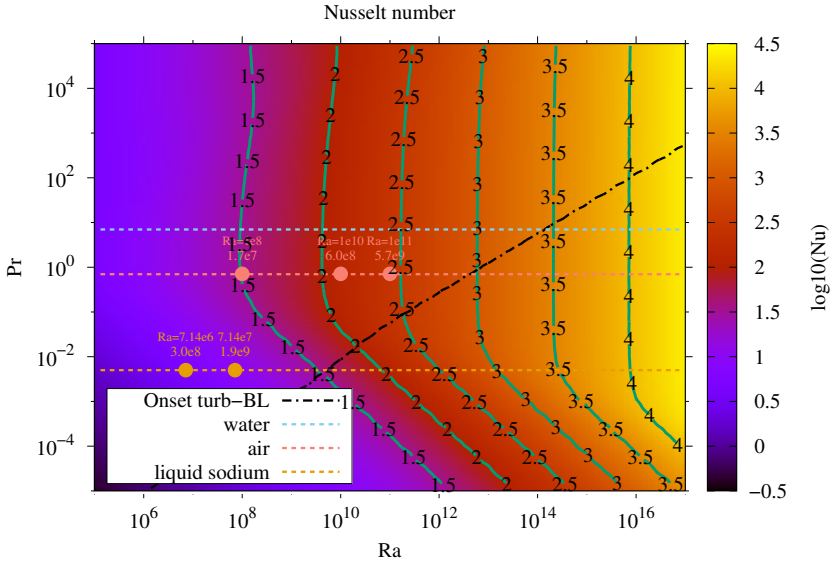

Figure 2: Estimation of the Nusselt number of a RBC in the $\{Ra, Pr\}$ phase space given by the classical GL theory [2] and its subsequent corrections [3]. Green solid isolines represent the $log10$ of the Nusselt. Three dashed horizontal lines correspond to three different working fluids: water ($Pr = 7$), air ($Pr = 0.7$) and liquid sodium ($Pr = 0.005$). Dots displayed correspond to the DNS simulations carried out in previous studies [5, 7, 8]. Black dash-dotted line is an estimation for the onset of turbulence in the thermal boundary layer.

walls, isothermal horizontal walls, perfectly smooth surfaces...) is a very hard task; therefore, the observation of the Kraichnan regime also remains elusive [3, 4].

2. LES of buoyancy-driven turbulence

2.1 Antecedents and failure of the eddy-diffusivity models

In this context, we may turn to large-eddy simulation (LES) to predict the large-scale behavior of incompressible turbulent flows driven by buoyancy at very high *Ra*-numbers. In LES, the

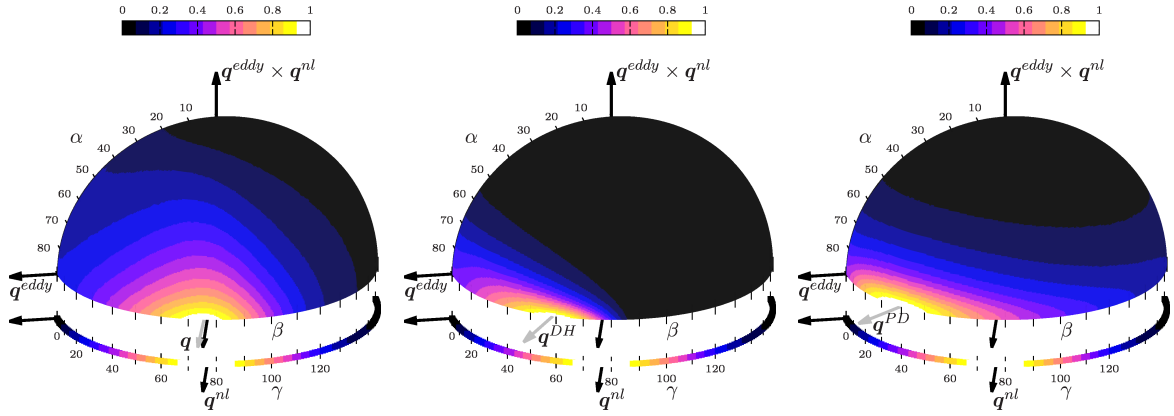

Figure 3: Joint probability distribution functions (PDF) of the angles (α, β) plotted on a half unit sphere to show the orientation in the space of the mixed model [9]. From left to right, alignment trends of the actual SGS heat flux, q, the Daly and Harlow [10] model and the Peng and Davidson [11] model. For simplicity, the JPDF and the PDF magnitudes are normalized by its maximal. For details the reader is referred to Ref. [12].

large-scale motions are explicitly computed, whereas the effects of small-scale motions are modeled. Since the advent of CFD, many subgrid-scale (SGS) models have been proposed and successfully applied to a wide range of flows [13]. However, there still exits inherent difficulties in the proper modelization of the SGS heat flux. This was analyzed in detail in the PRACE project entitled "*Exploring new frontiers in Rayleigh-Bénard convection*" (33.1Mh on MareNostrum 4), where DNS simulations of air-filled ($\mathrm{Pr} = 0.7$) RBC up to $Ra = 10^{11}$ were carried out using meshes up to 5600M grid points (see dots at $\mathrm{Pr} = 0.7$ displayed in Figure 2 and Figure 5, top). These results shed light into the flow topology and the small-scale dynamics which are crucial in constructing the turbulent wind and energy budgets [7]. Moreover, it also provided new insights into the preferential alignments of the SGS and its dependence with the Ra-numbers [8], highlighting that the modelization of the SGS heat flux is the main difficulty that (still) precludes reliable LES of buoyancy-driven flows at (very) high Ra-numbers.

Shortly, LES equations arise from applying a spatial commutative filter, $\overline{(\cdot)}$, with filter length δ, to the incompressible Navier-Stokes and thermal energy equations,

$$\frac{\partial \overline{u}}{\partial t} + (\overline{u}\cdot\nabla)\overline{u} = \sqrt{\frac{\mathrm{Pr}}{Ra}}\nabla^2\overline{u} - \nabla\overline{p} + \overline{f} - \nabla\cdot\tau, \tag{1}$$

$$\frac{\partial \overline{T}}{\partial t} + (\overline{u}\cdot\nabla)\overline{T} = \frac{1}{\sqrt{\mathrm{Pr}\,Ra}}\nabla^2\overline{T} \qquad -\nabla\cdot q, \tag{2}$$

where $\overline{u}$, $\overline{T}$ and $\overline{p}$ are respectively the filtered velocity, temperature and pressure, and the incompressibility constraint reads $\nabla\cdot\overline{u} = 0$. The SGS stress tensor, $\tau = \overline{u\otimes u} - \overline{u}\otimes\overline{u}$, and the SGS heat flux vector, $q = \overline{uT} - \overline{u}\,\overline{T}$, represent the effect of the unresolved scales, and they need to be modeled in order to close the system. The most popular approach is the eddy-viscosity assumption, where the SGS stress tensor is assumed to be aligned with the local rate-of-strain tensor, $\mathrm{S} = 1/2(\nabla\overline{u} + \nabla\overline{u}^t)$, *i.e.* $\tau \approx -2\nu_e \mathrm{S}(\overline{u})$.

By analogy, the SGS heat flux, q, is usually approximated using the gradient-diffusion hypothesis (linear modeling), given by

$$q \approx -\kappa_t \nabla \overline{T} \qquad (\equiv q^{eddy}). \tag{3}$$

Then, the Reynolds analogy assumption is applied to evaluate the eddy-diffusivity, κ_t, via a constant turbulent Prandtl number, Pr_t, *i.e.* $\kappa_t = \nu_e / Pr_t$. These assumptions have been shown to be erroneous to provide accurate predictions of the SGS heat flux [12, 9, 14]. Namely, *a priori* analysis showed that the eddy-diffusivity assumption, q^{eddy} (Eq. 3), is completely misaligned with the actual subgrid heat flux, q (see Figure 3, left). In contrast, the tensor diffusivity (non-linear) Leonard model [15], which is obtained by taking the leading term of the Taylor series expansion of q,

$$q \approx \frac{\delta^2}{12} \mathsf{G} \nabla \overline{T} \qquad (\equiv q^{nl}), \tag{4}$$

provides a much more accurate *a priori* representation of q (see Figure 3, left). Here, $\mathsf{G} \equiv \nabla \overline{u}$ represents the gradient of the resolved velocity field. It can be argued that the rotational geometries are prevalent in the bulk region over the strain slots, *i.e.* $|\Omega| > |\mathsf{S}|$ (see Refs [12, 5]). Then, the dominant anti-symmetric tensor, $\Omega = 1/2(\mathsf{G} - \mathsf{G}^*)$, rotates the thermal gradient vector, $\nabla \overline{T}$, to be almost perpendicular to q^{nl} (see Eq.4). Hence, the eddy-diffusivity paradigm is only valid in the not-so-frequent strain-dominated areas.

2.2 LES at very low Prandtl numbers

This inherent difficulty can be by-passed by carrying out simulations at low-Prandtl numbers. In this case, the ratio between the Kolmogorov length scale and the Obukhov-Corrsin length scale (the smallest scale for the temperature field) is given by $Pr^{3/4}$; therefore, for instance, at $Pr = 0.005$ (liquid sodium) we have a separation of more than one decade. Hence, it is possible to combine an LES simulation for the velocity field (momentum equation) with the numerical resolution of all the thermal scales. Results displayed in Figure 4 seem to confirm the adequacy of eddy-viscosity models for this kind of flows. Namely, Figure 4 (left) shows the Nusselt number for a set of meshes and eddy-viscosity models: the WALE model [16], the Vreman model [17], the QR model [18] and the S3QR model [19]. Results obtained without SGS model are also shown to illustrate the effect of the eddy-viscosity models to improve the solution. At first sight it can be observed that, in general, all LES solutions are in rather good agreement with the DNS data even for the coarsest grids ($48 \times 26 \times 26$ for $Ra = 7.14 \times 10^6$ and $96 \times 52 \times 52$ for $Ra = 7.14 \times 10^7$ whereas only the finest ones ($128 \times 72 \times 72$ and $192 \times 104 \times 104$ at $Ra = 7.14 \times 10^6$ and $512 \times 288 \times 288$ at $Ra = 7.14 \times 10^7$) can provide accurate results when the model is switched off. A closer inspection shows that slightly better results are obtained for those eddy-viscosity models (WALE and S3QR) that have the proper near-wall behavior, *i.e.* $\nu_e = \mathscr{O}(y^3)$. To emphasize the benefits of LES modeling, the approximate computational cost of the simulations is displayed in the top horizontal axis of Figure 4 (left): it was measured on the MareNostrum 4 supercomputer and corresponds to a total integration period of 500 time-units. Finally, to see the effect of eddy-viscosity models in more detail, results for the average turbulent kinetic energy are shown in Figure 4 (right) for two meshes and two eddy-viscosity models (WALE and S3QR). All these results seem to confirm the suitability of the eddy-viscosity assumption for buoyancy-driven flows. For more details the reader is referred to Ref. [8].

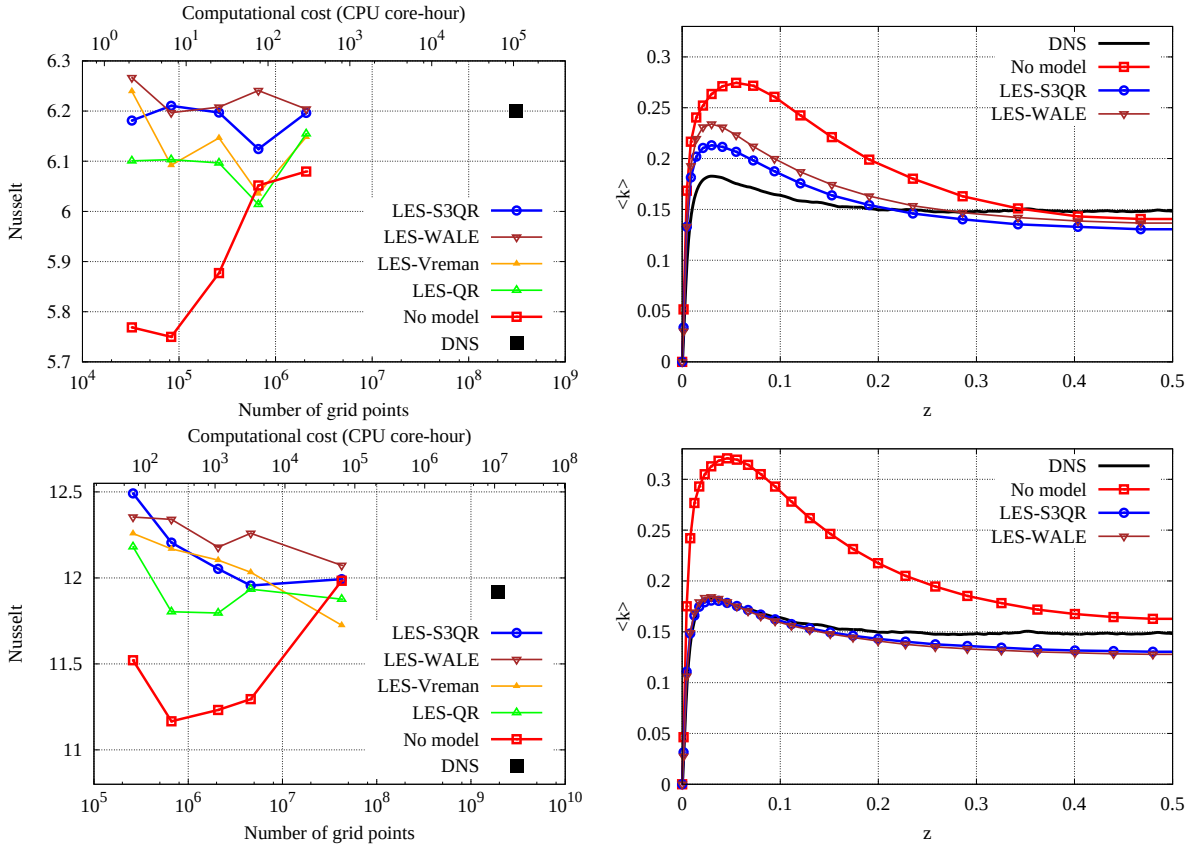

Figure 4: Comparison of LES (and no-model) versus DNS results of liquid-sodium ($Pr = 0.005$) RBC at $Ra = 7.14 \times 10^6$ and 7.14×10^7. Left: average Nusselt for different meshes at $Ra = 7.14 \times 10^6$ (top) and $Ra = 7.14 \times 10^7$ (bottom). Corresponding computational costs at the MareNostrum 4 supercomputer are shown in the top of the plots. Right: LES results of turbulent kinetic energy at cavity mid-width for a $64 \times 36 \times 36$ (top) and $96 \times 52 \times 52$ (bottom) meshes compared with the DNS results obtained with a mesh of $488 \times 488 \times 1280 \approx 305M$.

3. Preliminary results and conclusions

The results presented in the previous section confirm that low-Pr LES simulations are able to provide accurate predictions of the overall Nu with meshes significantly coarser than for DNS (*e.g.* in practice for $Pr = 0.005$ we can expect mesh reductions in the range 10^2-10^3 for the total number of grid points). This can be clearly observed in Figure 5 (bottom), where estimations of the mesh size for LES are given with the assumption that thermal scales are fully resolved. This huge gain becomes even more evident in Figure 6 where the number of CPU-core hours (on the basis of MareNostrum 4 supercomputer) is estimated both for DNS and LES. In this case, the difference between DNS and LES goes up to $\mathscr{O}(10^4)$ due to the fact that not only the mesh resolution decreases but also the total number of time-steps. Nowadays, the typical size of a Tier-0 project is $\mathscr{O}(10^8)$ hours. Therefore, according to the estimations displayed in Figure 6, the so-called ultimate regime of turbulence can be potentially reached carrying out LES at low-Pr using meshes of 10^{10}-10^{11} grid points.

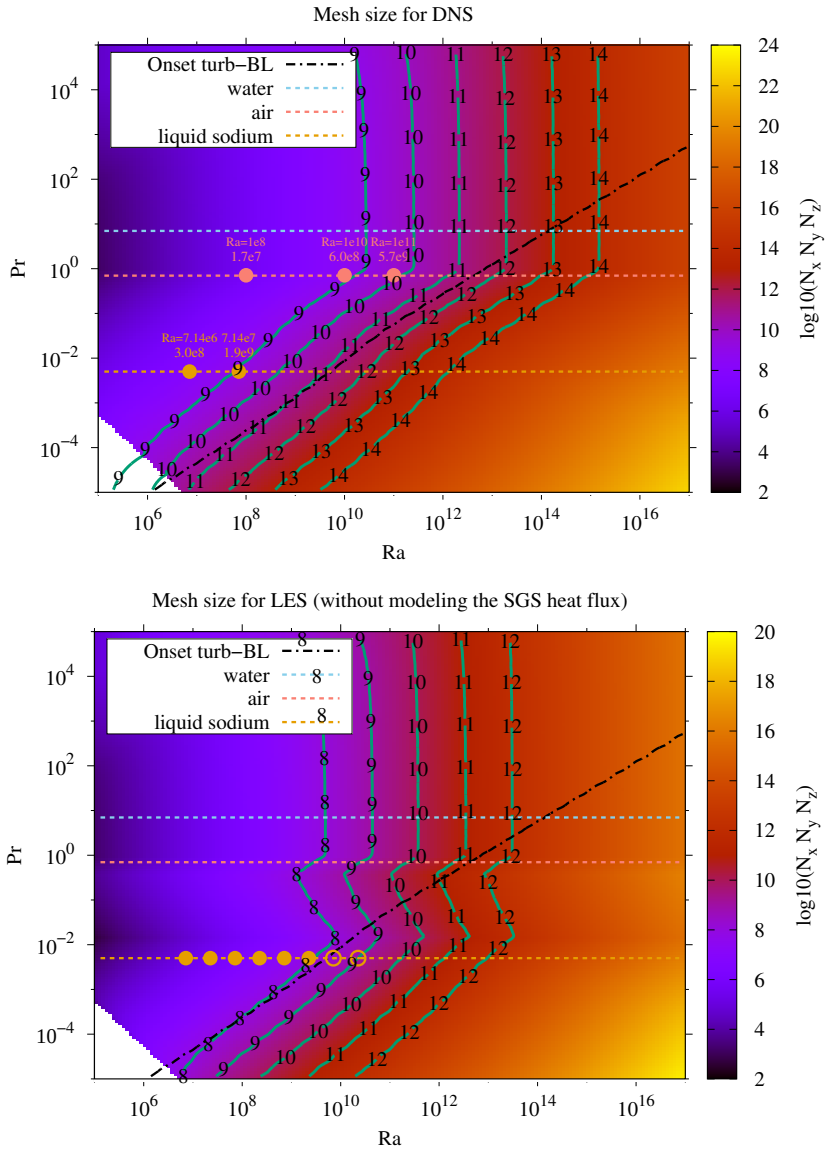

Figure 5: Estimation of the mesh sizes for DNS (top) and LES (bottom) simulations of RBC in the $\{Ra, Pr\}$-phase space. LES estimations assume that thermal scales are fully resolved, *i.e.* no SGS heat flux model is needed. Green solid isolines represent the $log10$ of the total number of grid points. Three dashed horizontal lines correspond to three different working fluids: water ($Pr = 7$), air ($Pr = 0.7$) and liquid sodium ($Pr = 0.005$). Dots displayed in the left figure correspond to the DNS simulations carried out in previous studies [5, 7, 8] whereas the dots shown in the bottom figure are the set of LES simulations (being) carried out in the present work. Black dash-dotted line is an estimation for the onset of turbulence in the thermal boundary layer.

In this regard, a set of LES simulations of RBC at $Pr = 0.005$ for a wide range of Ra numbers (see dots in Figure 5, bottom) are being carried out on MareNostrum 4 supercomputer. The configuration is the same as in Ref.[8] where two DNS simulations (solid black dots in

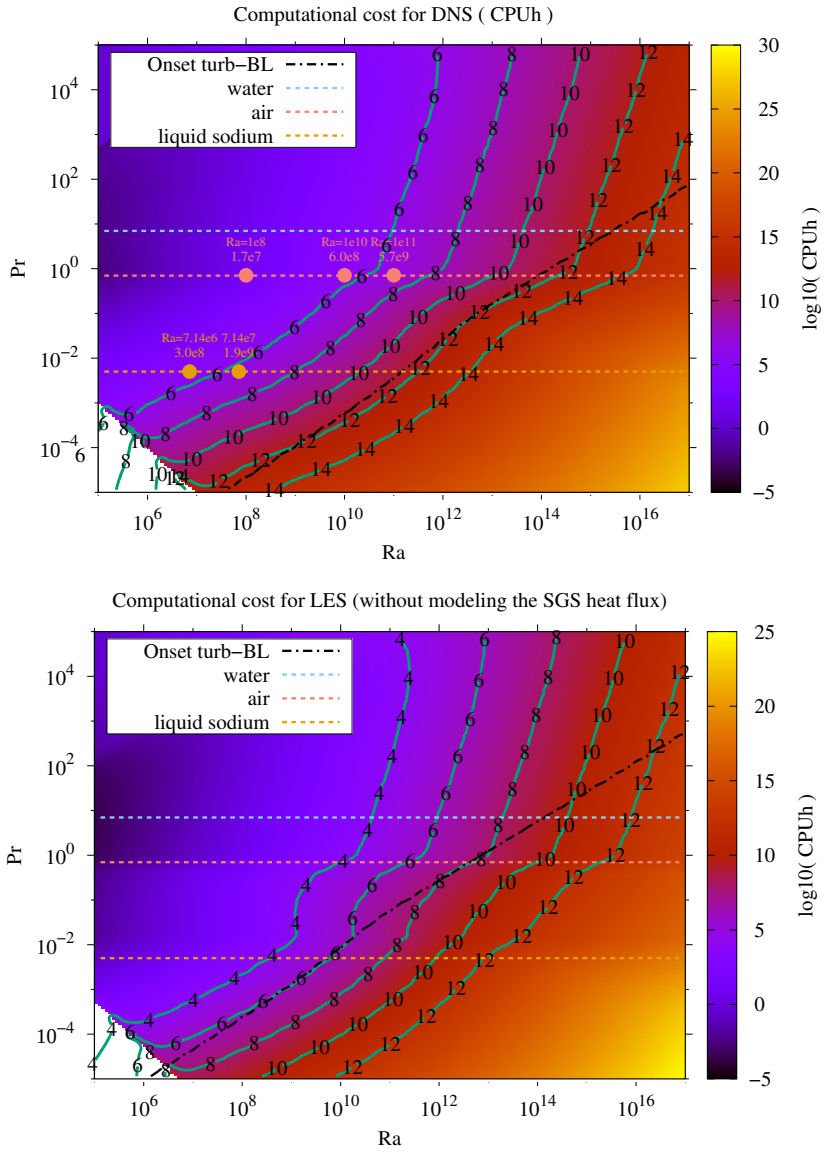

Figure 6: Same as in Figure 5 but for the cost of simulations in CPU-core hours. Estimations done for the MareNostrum 4 supercomputer at the Barcelona Supercomputing Center. Each computing node has two Intel Xeon 8160 (24 cores, 2.1 GHz, 33 MB L3 cache and 128 GB/s memory bandwidth) linked to 96GB of RAM and interconnected through 12.5 GB/s Intel Omni-Path. Overall computational cost corresponds to 500 time-units.

Figure 7) were computed using meshes with $488 \times 488 \times 1280 \approx 305M$ ($Ra = 7.14 \times 10^6$) and $996 \times 996 \times 2048 \approx 1911M$ ($Ra = 7.14 \times 10^7$) grid points, respectively. For the LES simulations, two levels of mesh refinement are being used: namely, a fine level that approximately corresponds to estimations shown in Figure 5 (bottom) and a coarse level which is approximately twice coarser in each spatial direction. For instance, LES meshes at $Ra = 7.14 \times 10^7$ have respectively $44 \times 44 \times 96 \approx 0.19M$ and $90 \times 90 \times 160 \approx 1.3M$ grid points, *i.e.* ≈ 10000 and ≈ 1500 coarser compared with the DNS mesh. Meshes are designed to properly resolve the boundary layer whereas the much coarser bulk region is fine enough to guarantee that thermal

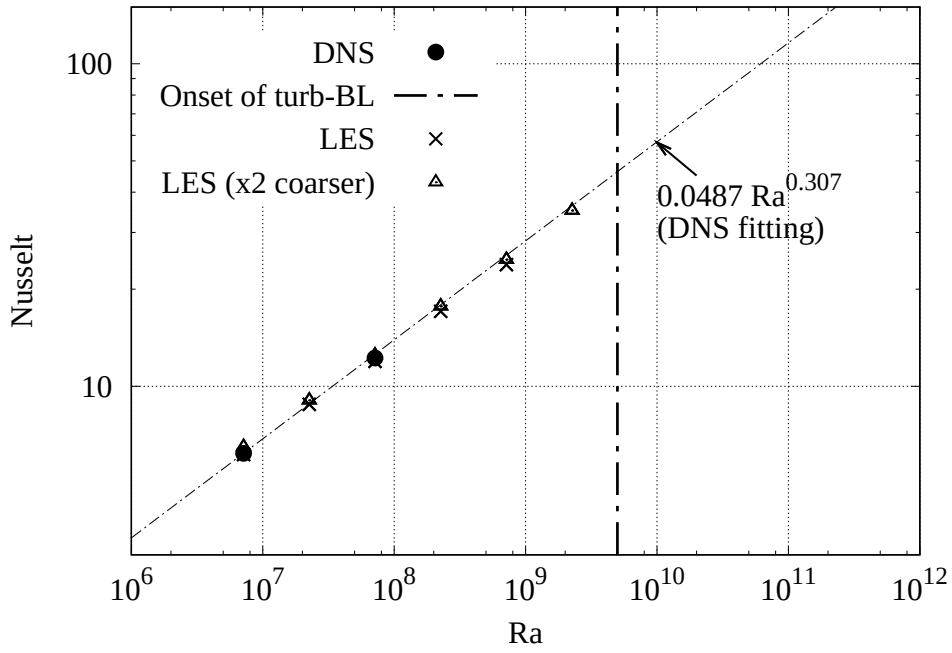

Figure 7: *Nu*-vs-*Ra* results obtained with LES at $Pr = 0.005$ using the same RBC configuration as in Ref.[8] where the two DNS results (solid black dots) were computed. The vertical dash-dotted line corresponds to the estimated *Ra* (for this particular *Pr*) where the thermal boundary layer becomes turbulent.

scales are fully resolved, *i.e.* no SGS heat flux model is needed. Then, the SGS stress tensor is modeled using the S3PQ model [19] which was already tested for this RBC configuration in oru previous work [8].

Results of the overall Nusselt number are displayed in Figure 7. LES simulations up to $Ra = 7.14 \times 10^{10}$ (for the coarse level) and $Ra = 2.26 \times 10^{10}$ (for the fine level) are still being computed on MareNostrum 4 supercomputer. These points are located beyond the transition point for this *Pr*-number (see Figure 5, right). Nevertheless, these simulations are not statistically converged yet and, therefore, results are not shown here. At first sight, we can observe an accurate agreement with previous DNS results. Furthermore, there is a rather good agreement with the *Nu*-vs-*Ra* scaling predicted using the DNS data. In any case, these preliminary results show the capability to obtain accurate predictions of the *Nu*-number using LES simulations. Accordingly to the classical GL theory, on-going LES simulations at higher *Ra*-number should possibly show a change in the *Nu*-vs-*Ra* scaling indicating that we are finally hitting the ultimate regime of thermal turbulence.

Extending these studies to finer grids and higher *Ra* numbers is part of our near future research plans. Furthermore, these (large-scale) simulations should run efficiently on the variety of modern HPC systems (CPUs, GPUs, ARM,...) while keeping the code easy to port and maintain. In this regard, our *leitmotiv* reads: relying on a minimal set of (algebraic) kernels [20, 21] (*e.g.* sparse-matrix vector product, SpMV; dot product; linear combination of vectors) is crucial for an efficient cross-platform portability and optimization.

Acknowledgments

F.X.T. and A.O. are supported by the *Ministerio de Economía y Competitividad*, Spain, RETOtwin project (PDC2021-120970-I00). Calculations were carried out on the MareNostrum 4 supercomputer at BSC. We thankfully acknowledge these institutions.

References

1. R. J. A. M. Stevens, , D. Lohse, and R. Verzicco. Toward DNS of the Ultimate Regime of Rayleigh–Bénard Convection. In *Direct and Large Eddy Simulation XII*, pages 215–224, Madrid, Spain, 2019. Springer International Publishing.
2. S. Grossmann and D. Lohse. Scaling in thermal convection: a unifying theory. *Journal of Fluid Mechanics*, 407:27–56, 2000.
3. R. J. A. M. Stevens, E. P. van der Poel, S. Grossmann, and D. Lohse. The unifying theory of scaling in thermal convection: the updated prefactors. *Journal of Fluid Mechanics*, 730:295–308, 2013.
4. S. Bhattacharya, M. K. Verma, and R. Samtaney. Revisiting Reynolds and Nusselt numbers in turbulent thermal convection. *Physics of Fluids*, 33:015113, 2021.
5. F. Dabbagh, F. X. Trias, A. Gorobets, and A. Oliva. On the evolution of flow topology in turbulent Rayleigh-Bénard convection. *Physics of Fluids*, 28:115105, 2016.
6. R. H. Kraichnan. Turbulent thermal convection at arbitrary Prandtl number. *Physics of Fluids*, 5:1374–1389, 1962.
7. F. Dabbagh, F. X. Trias, A. Gorobets, and A. Oliva. Flow topology dynamics in a three-dimensional phase space for turbulent Rayleigh-Bénard convection. *Physical Review Fluids*, 5:024603, 2020.
8. F.X. Trias, F.Dabbagh, A.Gorobets, and C.Oliet. On a proper tensor-diffusivity model for large-eddy simulation of buoyancy-driven turbulence. *Flow, Turbulence and Combustion*, 105:393–414, 2020.
9. C. W. Higgins, M. B. Parlange, and C. Meneveau. The heat flux and the temperature gradient in the lower atmosphere. *Geophysical Research Letter*, 31:L22105, 2004.
10. B. J. Daly and F. H. Harlow. Transport equations in turbulence. *Physics of Fluids*, 13:2634, 1970.
11. S. Peng and L. Davidson. On a subgrid-scale heat flux model for large eddy simulation of turbulent thermal flow. *International Journal of Heat and Mass Transfer*, 45:1393–1405, 2002.
12. F. Dabbagh, F. X. Trias, A. Gorobets, and A. Oliva. A priori study of subgrid-scale features in turbulent Rayleigh-Bénard convection. *Physics of Fluids*, 29:105103, 2017.
13. P. Sagaut. *Large Eddy Simulation for Incompressible Flows: An Introduction*. Springer, 3^{rd} edition, 2005.
14. S. G. Chumakov. "*A priori* study of subgrid-scale flux of a passive scalar in isotropic homogeneous turbulence. *Physical Review E*, 78:036313, 2008.
15. A. Leonard. Large-eddy simulation of chaotic convection and beyond. *AIAA paper*, 97-0304, 1997.
16. F. Nicoud and F. Ducros. Subgrid-scale stress modelling based on the square of the velocity gradient tensor. *Flow, Turbulence and Combustion*, 62(3):183–200, 1999.
17. A. W. Vreman. An eddy-viscosity subgrid-scale model for turbulent shear flow: Algebraic theory and applications. *Physics of Fluids*, 16(10):3670–3681, 2004.

18. R. Verstappen. When does eddy viscosity damp subfilter scales sufficiently? *Journal of Scientific Computing*, 49(1):94–110, 2011.
19. F. X. Trias, D. Folch, A. Gorobets, and A. Oliva. Building proper invariants for eddy-viscosity subgrid-scale models. *Physics of Fluids*, 27(6):065103, 2015.
20. X. Álvarez, A. Gorobets, F. X. Trias, R. Borrell, and G. Oyarzun. HPC^2 - a fully portable algebra-dominant framework for heterogeneous computing. Application to CFD. *Computers & Fluids*, 173:285–292, 2018.
21. X. Álvarez, A. Gorobets, and F. X. Trias. A hierarchical parallel implementation for heterogeneous computing. Application to algebra-based CFD simulations on hybrid supercomputers. *Computers & Fluids*, 214:104768, 2021.